Engineering Geology xxx (xxxx) xxx

Contents lists available at ScienceDirect

Engineering Geology

journal homepage: www.elsevier.com/locate/enggeo

When faults diverge – High resolution imaging of an intra-fault zone in an urban environment. A case study from the city of Tiberias, Israel

Michael Lazar [a,*], Uri Basson [a,b], Ram Ben-David [c], Judah Coddington [c]

[a] Dr. Moses Strauss Department of Marine Geosciences, University of Haifa, Mount Carmel, Haifa 31905, Israel
[b] GeoSense Ltd., 24 Natan Yonatan St., Netanya 4266010, Israel
[c] Roved Geology and Social Consultancy Ltd, PO Box 128, Givat Yeshayahu 9982500, Israel

ARTICLE INFO

Keywords:
Ground penetrating radar
Building codes
Active faults
Potentially active faults

ABSTRACT

The presence of active faults or potentially active faults in urban settings is of great concern to city planners and developers. The high value of property within cities means that it is not always possible to avoid construction in such areas. Thus, building codes exist in order to regulate where and how to build in the vicinity of such faults. The Israeli National Building Code defines a *zone of active faulting* as a 200-m wide area on each side of an active or potentially active fault trace. In this area, there is a high potential for repeated activity of undetected branches or secondary faults and construction should be avoided or built with extreme safety measures in place. The current study examines an area located between two fault strands – an active and a potentially active one - in the city of Tiberias, northern Israel. The area lies outside the active fault zones defined for each strand (i.e., at a distance of more than 200 m from each fault). Eight high-resolution ground penetrating radar (GPR) profiles were collected along the streets that crisscross this area. Results show a dense series of potential fault strands that reach the base of the artificial fill that was laid down for the construction of the roads, indicating potential seismic hazard in this seemingly "safe" zone, thus raising a "red flag" for construction plans in the area. A geological study should be conducted to validate the geophysical results. This study shows the importance in conducting a geophysical site survey in tectonically active settings, even in areas that lie outside well defined zones of active faulting.

1. Introduction

Although first approved in 1980, the Israel *Standard SI-413: Design provisions for* earthquake resistance of structures was fully implemented only in 1995 by the Israel Institute of Standards as part of the National Building Code (Shohet et al., 2016). As such, it is strictly observed and enforced. Amendment No. 5 to Standard SI-413 is the last document whose draft is freely available online (Standards Institute, 2013). According to Section 103.36 of the Amendment, an active fault is "A fault that was defined by the Institution of Geology as an active fault and appears in the updated map of active faults and faults that are suspected as potentially fault active in Israel". Similarly, section 103.37 goes on to define a Potentially Active fault as one that lacks proof of activity, but appears on the map of the Geological Institute of Israel and adheres to their definition of such a fault. These definitions were expanded upon by Sagy et al. (2017) who defined an active fault as one that has ruptured the surface at least once in the last 13,000 years. They also definedpotentially active faults as either a direct branch of an active fault or one that has ruptured the surface at least once between 35,000 to 13,000 years before present. Finally, Section 103.38 defines a zone of active faulting as a 200-m wide area on each side of the active or potentially active fault trace. Within the boundaries of these areas, there is a high potential for repeated activity of undetected branches or secondary faults.

Other tectonically active areas use similar definitions. In California for example (Bryant and Hart, 2007), the Alquist-Priolo Earthquake Fault Zoning (APEFZ) Act was initiated in order to avoid construction of buildings across traces of active faults and by this, mitigate the threat of surface rupture to structures assigned for human occupancy. According to this Act, active faults are defined as those along which motion has occurred within the last 11,000 years and defined as active by Polices and Criteria of the State Mining and Geology Board. Earthquake Fault Zones (EFZ), the equivalent of the Israeli zones of active faulting, are located 500 ft (150 m) away from major active faults and 200–300 ft

* Corresponding author.
E-mail address: mlazar@univ.haifa.ac.il (M. Lazar).

https://doi.org/10.1016/j.enggeo.2021.106454
Received 1 August 2021; Received in revised form 29 October 2021; Accepted 6 November 2021
Available online 11 November 2021

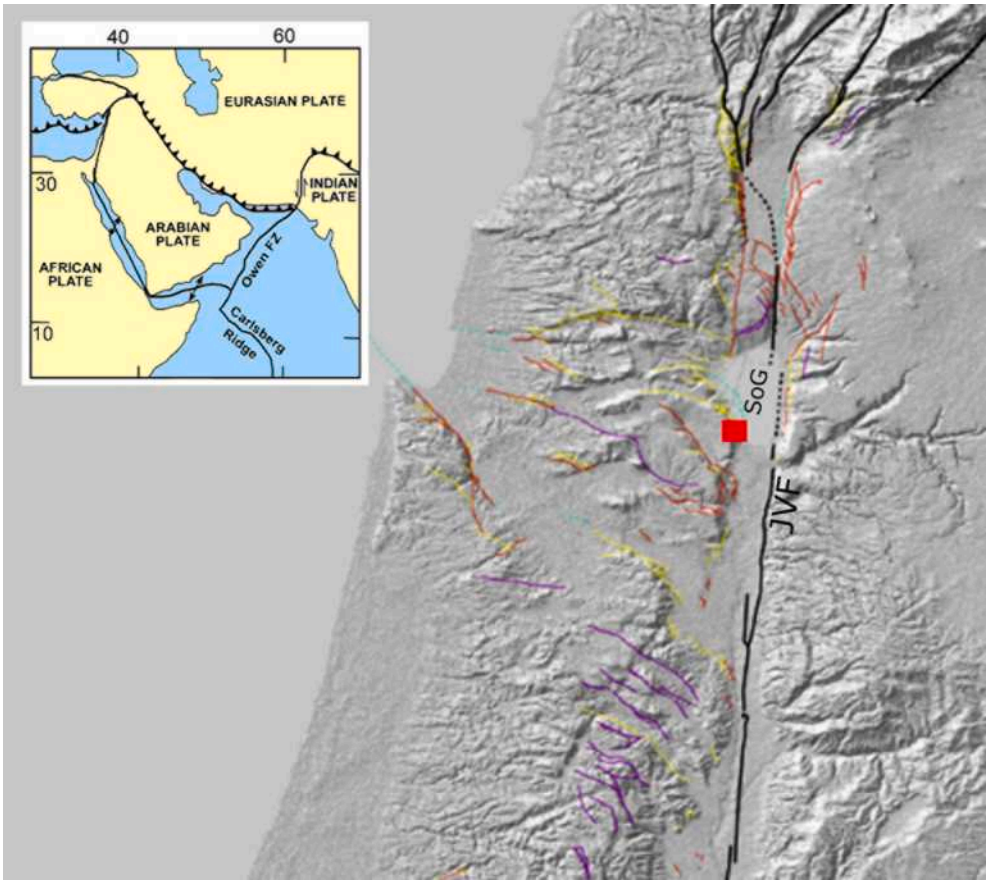

Fig. 1. Tectonic map showing: main strike slip segment of the Dead Sea fault (solid black line, dashed where inferred); lineaments showing evidence of Quaternary activity (red); marginal faults and main branches (yellow); >6 km segments associated with recent seismicity (purple) and subsurface or inferred faults (turquoise). After Sharon et al., 2020. Red box marks the location of the study area shown in Fig. 2. JVF – Jordan Valley Fault. SoG – Sea of Galilee, Inset – general tectonics of the eastern Mediterranean and its surroundings. (For interpretation of the references to color in this figure legend, the reader is referred to the web version of this article.)

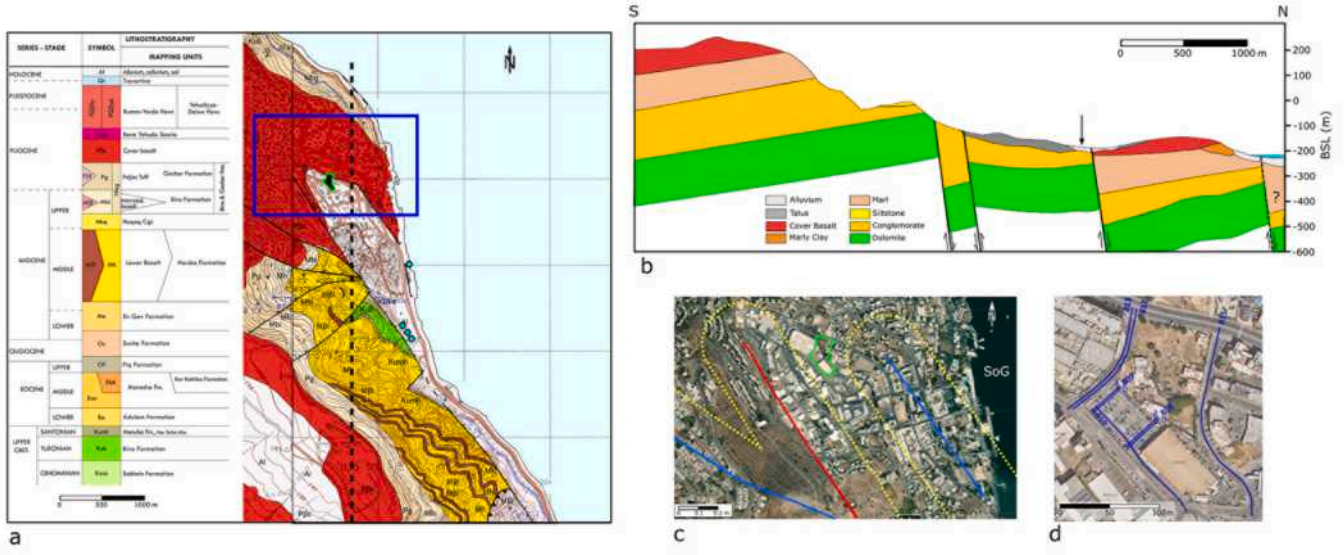

Fig. 2. Location maps showing (a) the geological map of the area (after Bogoch and Sneh, 2008 and Sneh, 2008). The dashed black line mark the location of the profile presented in (b), while colors correspond to the legend. Blue rectangle marks the study area shown in (c). Black-filled green polygon marks the location of the geophysical survey presented in (d). Turquoise circles are evidence for surface rupture as mapped by Ferrario et al. (2020). (b) geological cross-section through the City of Tiberias south of the study area (after Zaslavsky et al., 2009). Colors correspond to legend presented in (a) (c) the southeastern section of the city of Tiberias. The study area is marked by a green polygon. Red line marks active faults, Blue – possibly active faults. Dashed yellow line is the 200 m zone of active faulting around active and potentially active faults. SoG – Sea of Galilee. Modified from the Geological Survey of Israel online database (Rosensaft and Sagy, 2019). (d) Close up of the study area showing the location of the GPR profiles collected for this study. (For interpretation of the references to color in this figure legend, the reader is referred to the web version of this article.)

(60–90 m) away from well-defined minor faults.

On the other hand, a more "forgiving" approach was adopted in New Zealand. According to King et al. (2003) a "control zone" is defined as an area that extends 20 m to either side of a "fault zone" (expressed as an zone of ground damage). This is considered to be an area of potential activity where building should be avoided (PCE, 2001).

The current study focuses on the city of Tiberias along the southwestern shore of the Sea of Galilee, northern Israel (Fig. 1). It examines an area that lies outside the 200 m zone of potentially active faulting of two fault branches that cut through the western limits of the city.

2. Geological and tectonic background

Little geological information is readily available for the modern-day city of Tiberias. The geological map is presented in Fig. 2a. A general cross section that cuts near the study area was provided by Zaslavsky et al. (2009) based on H/V spectral ratio analysis (the spectral ratio of the horizontal versus the vertical component of motion) extracted from microtremor measurements and from borehole data (Fig. 2b). According to this analysis, the Albian to Turonian (~110–90 ma BP) Judea Group comprises the lowest stratigraphic unit and consists mainly of limestone and dolomite. Above this lies the terrestrial Early Miocene conglomerate, chalk and limestone with alternating basalt layers (the Lower Basalt) of the Hordus and Hoquq Fms. This is topped by the Late Pliocene to Early Pliocene (~7–3 ma BP) Bira and Gesher Fms composed of marl, clay and chalk layers. Finally, a Mid-Pliocene to Lower Pleistocene phase of volcanism (the Cover Basalt) covered the entire area and into Syria. According to the cross-section, specifically in the study area, the Bira and Gesher Fms are missing, as well as the Cover Basalt. The Hordus Fm. and the Huquq Conglomerate are topped by recent Holocene alluvium as evident also in the geological map. The Cover Basalt is present at the northern end of the study area. Further to the south and outside the study area, evidence for landslide deposits (talus) is present. Such a geological setting, where soft sediments overlie stiff rocks with higher seismic velocities, can generate local ground motion amplification during an earthquake.

The Sea of Galilee (Lake Kinneret) is a pull-apart basin in northern Israel that was formed as a result of the active Dead Sea plate boundary, a strike-slip fault that separates the Africa/Sinai and Arabian plates (e.g., Hurwitz et al., 2002; Ben-Avraham et al., 2008) (Fig. 1). While the fault pattern within the lake is somewhat debated (see Gasperini et al., 2020 for a summary) the faults on land are more-or-less constrained. The main strand of the plate boundary, the sinistral Jordan Valley fault (Fig. 1), lies on the eastern shore of this freshwater lake (Marco et al., 2005; Hamiel et al., 2016; Wechsler et al., 2018 and reference therein). The western shore is cut by a series of normal faults that dip to the east (Fig. 1; Sneh and Weinberger, 2014; Sagy et al., 2016; Sharon et al., 2020). The easternmost of these faults cuts through the city of Tiberias and is considered potentially active. The general direction of the fault is northwest-southeast. According to Zaslavsky et al. (2009), the northern block (the hanging wall) is down dropping ca 100 m relative to the southern block (footwall). The fault is suspected to reach surface but due to artificial cover it is difficult to trace.

The area within the lake and its surroundings is characterized by low-level tectonic activity, which is occasionally pierced by destructive events. According to historical earthquake catalogues (Ambraseys and Melville, 1988) intense damage to areas around the Sea of Galilee, was caused by strong earthquakes occurring in 303, 363, 551, 749, 1202, 1759, and 1837 CE. More recently, two swarms of earthquakes were recorded in the lake itself, to the northwest. The 2013 M_L3.7 and 2018 M_L4.6 events (e.g. Wetzler et al., 2019; Gasperini et al., 2020; Haddad et al., 2020), both caused slight damage to buildings in the city of Tiberias, which lies on the southwestern shore of the lake (Fig. 1). It is the largest city in the region, covering an area of around 11 km^2 with an estimated population of ca. 45,000 inhabitants. Massive damage to the city was cause by numerous earthquakes, most notably a series of events occurring in the mid-8th century, which were attributed in the past to a single event (Marco et al., 2003; Ferrario et al., 2020) and the 1837 event (Ambraseys, 1997; Zohar, 2016). According to Wei et al. (2015), Tiberias has been damaged at least eleven times since its establishment in 19 CE, with earthquakes occurring every 150–185 years. This relatively long list of historical earthquakes shows the potential for active tectonics in the modern City of Tiberias. In addition, examination of archaeological evidence (Ferrario et al., 2020), stressed the potential of the faults that cut through Tiberias (south of the study area) as a major source of earthquakes that can cause surface rupture despite lack of instrumental evidence.

The Geological Survey of Israel maintains an updated map archive and interactive database of active and potentially active faults in the region (Rosensaft and Sagy, 2019). This provides the base for determining whether an area is safe for construction or not, in accordance with the regulations set down in SI 413 and the definitions in Amendment No. 5. For the current study, an area between the zone surrounding an active fault and the zone around a potentially active fault was examined in Tiberias using ground penetrating radar (GPR). Both faults cut through the city (Fig. 2c) and sit on Holocene alluvium (Sneh, 2008). The area examined in the current study falls outside the 200 m limited defined by Amendment No. 5 and thus should be free of seismic effects and "safer" for construction.

3. Methods

GPR has been applied in many different settings for various purposes and has been proven time and again as a reliable method for subsurface investigation (e.g. see Jol, 2009 and Utsi, 2017 for a summary). Specifically, the use of GPR for fault detection has been well established over the years (e.g. Basson et al., 1994; Grasmueck, 1996; Gross et al., 2000; Demanet et al., 2001; Basson et al., 2002; Rashed et al., 2003; Reiss et al., 2003; Maurya et al., 2005; Pauselli et al., 2010; Ercoli et al., 2013; Maurya et al., 2013; Ercoli et al., 2014; Zhang et al., 2019; Aliyannezhadi et al., 2020 - to name but a few studies) due to the extremely high-resolution of data obtained for the shallow subsurface. This makes it particularly useful for studies pertaining to shallow active faulting as opposed to other methods such as seismic reflection, which are limited in their ability to image the upper tens of meters of the subsurface in high resolution. The method itself uses the transmission of radar waves and provides imaging of the shallow subsurface down to depths ranging between several centimeters to tens of meters. Depth of penetration depends on the frequency of the antenna used to generate the electromagnetic waves, with lower frequencies penetrating deeper. Energy reflected by features with contrasting electrical impedance is recorded on the surface by the receiver. The amplitude, or strength of the return signal, is dependent on contrasts in the dielectric constant and electrical conductivity of the target and its surroundings. Differences in properties can be a result of changes in composition, porosity, conductivity, water content, etc. Interpretation of faults in GPR data is based on examination of offsets of reflections on both sides of the lineament, as expressed in both amplitude and phase diagrams. GRP reflectors also generally tend to warp towards faults and/or become discontinuous (e.g. Chow et al., 2001; Anderson et al., 2003; Jol, 2009).The survey conducted for this study was carried out using a Mala Ground Explorer (GX) system. This GPR system, produced by Mala Geoscience, uses High Dynamic Range (HDR) technology to create very high quality data recorded at 32 bit resolution. A central antenna frequency of 80 MHz was chosen in order to maximize penetration. This is the lowest frequency antenna available for this system. Sampling frequency was set to 960 MHz and samples were collected every 10 cm along each profile. The time window (the time between two transmitted pulses) was 420 ns with a stack of around 64 traces per sample. Data were collected along paved roads to minimize environmental interference in an urban area that has undergone massive construction during the last few years. A total of 765 m of data were collected along eight profiles (Fig. 2d). The

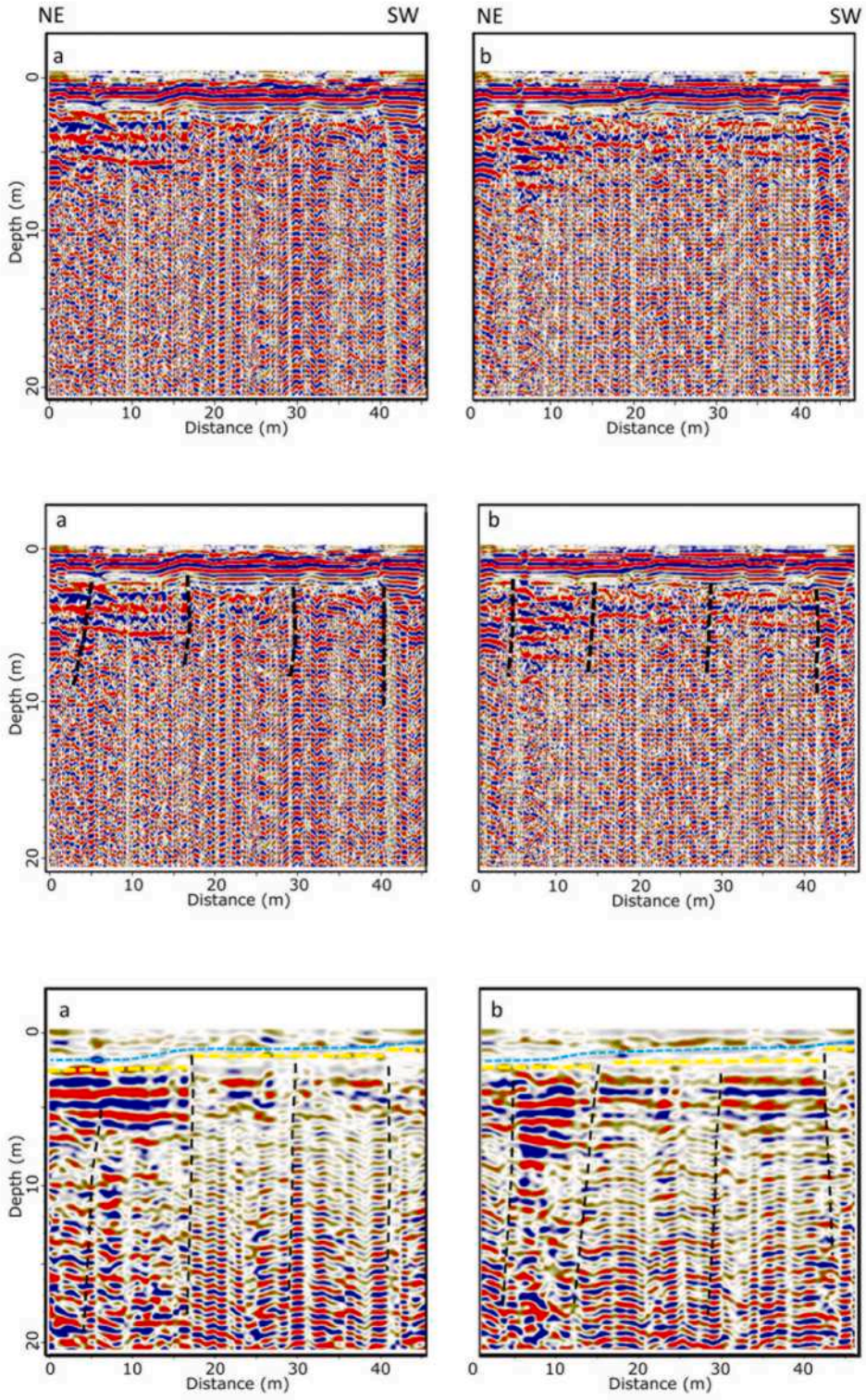

Fig. 3. Northeast-southwest GPR profiles 808a and 808b. Color scale represents the strength of reflection and phase. The top profile was processed to highlight the top meters. Middle profile is the same as top but with interpretation. The bottom profile was processed to highlight the deeper subsurface down to 20 m. Light blue dashed line marks the bottom of the infill, while yellow dashed lines represents faulted segments. (For interpretation of the references to color in this figure legend, the reader is referred to the web version of this article.)

advantage of using the HDR system lies in its large bandwidth. The low frequency used here allows maximum penetration (~20 m below the surface in this study). The wide dynamic range of the HDR system provides relatively good resolution of the shallower subsurface.

Data were processed using ReflexW and GroundVision software packages. Static corrections were preformed to adjust zero time to the ground surface and a topographic correction was applied to locate each trace in the correct location. Topographic slopes are rather uniform in the study area thus the figures are presented here without the correction. Signal drift and DC shift caused by very low frequencies were removed with a "Dewow" filter. Afterwards, a bandpass filter of 10–250 MHz was applied. Background removal (subtraction of an average trace) allowed for the removal of system noise, ground bounce, soil roughness scattering and reflection signals from external anomalies, which appear in the data as periodic ringing and nearly horizontal reflectors. Finally, an automatic gain control (AGC) function was used to enhance small

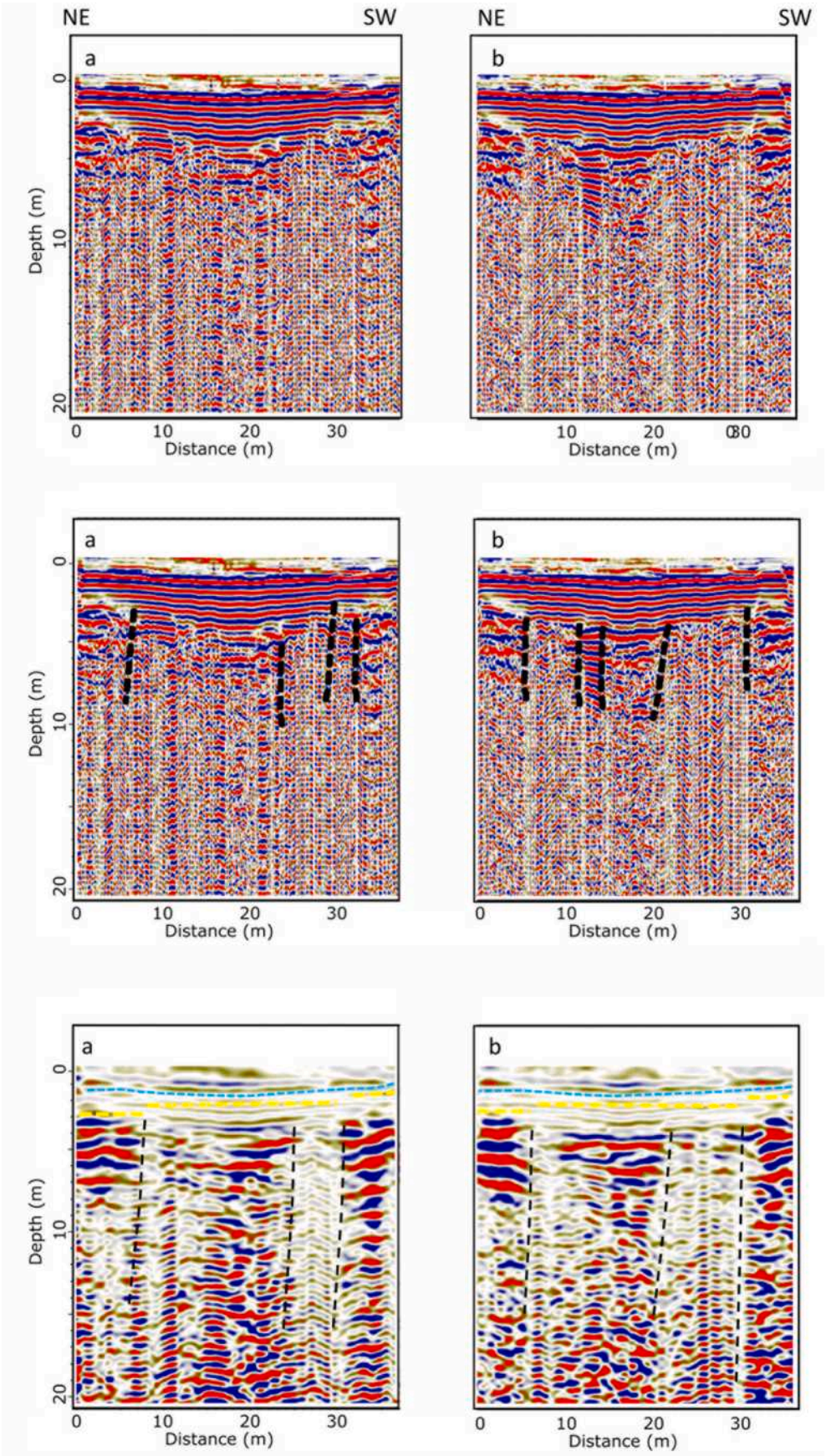

Fig. 4. Northeast-southwest GPR profiles 809a and 809b. Color scale represents the strength of reflection and phase. The top profile was processed to highlight the top meters. Middle profile is the same as top but with interpretation. The bottom profile was processed to highlight the deeper subsurface down to 20 m. Light blue dashed line marks the bottom of the infill, while yellow dashed lines represents faulted segments. (For interpretation of the references to color in this figure legend, the reader is referred to the web version of this article.)

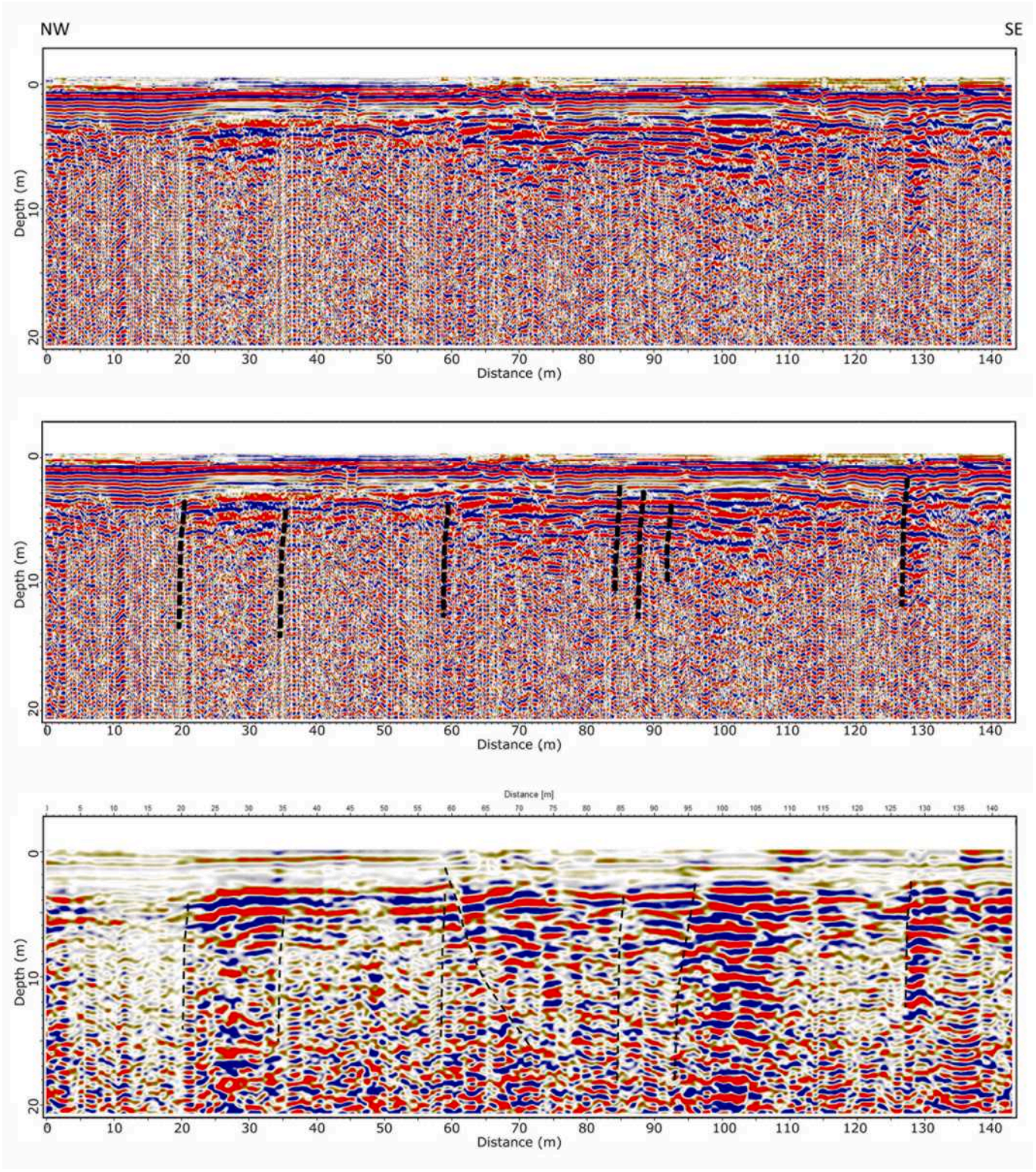

Fig. 5. Northwest-southeast GPR profile 810. Color scale represents the strength of reflection and phase. The top profile was processed to highlight the top meters. Middle profile is the same as top but with interpretation. The bottom profile was processed to highlight the deeper subsurface down to 20 m. Dashed black lines mark suspected faults mapped in this study.

amplitudes. Additional, advanced proprietary processing to improve the data was applied.

4. Results and discussion

Horizontal resolution of the data collected in this study can be defined as the First Fresnel zone and was calculated accordingly (Sheriff, 1980). The horizontal resolution was found to be 0.23 m - 0.38 m.

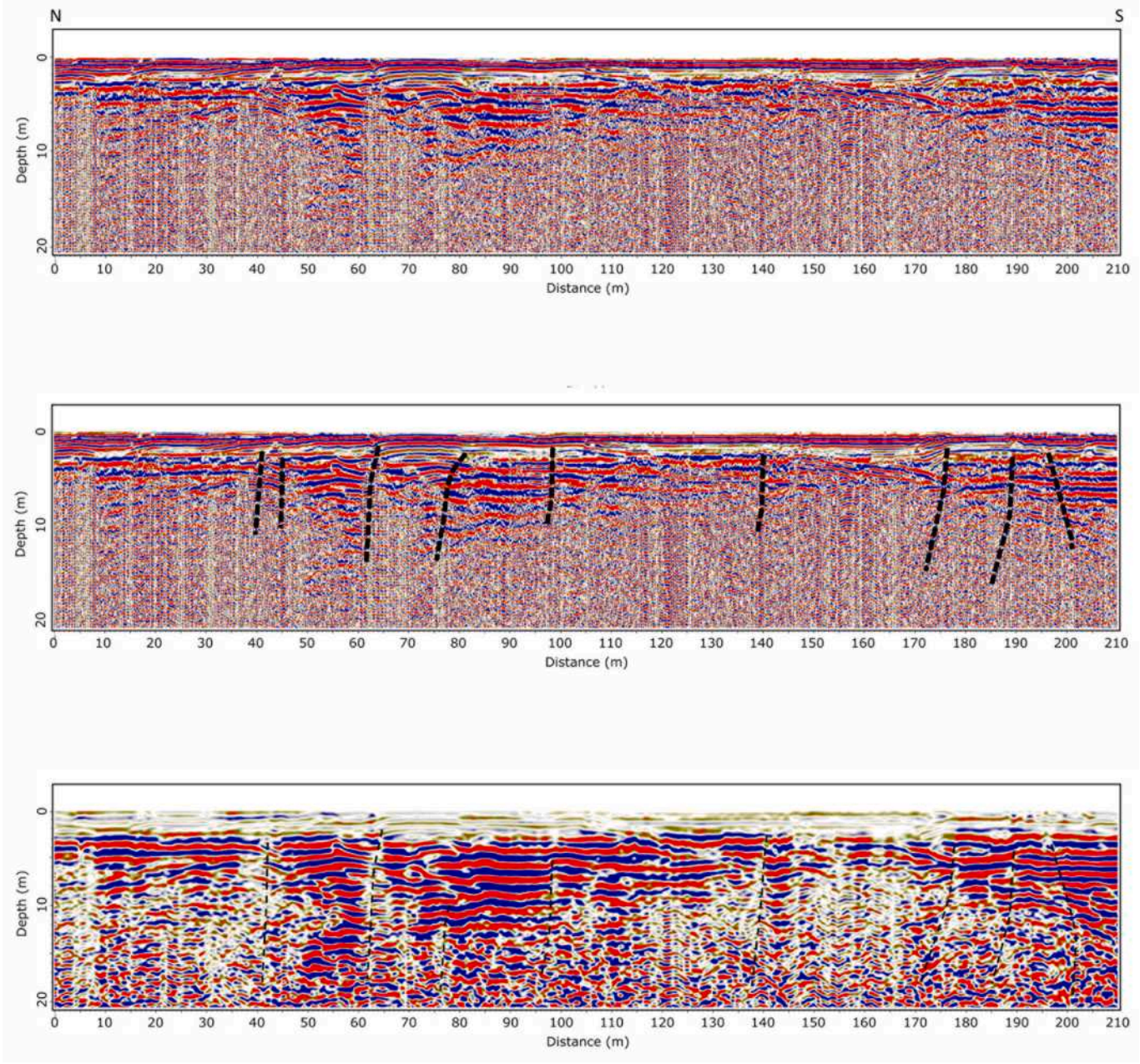

Fig. 6. North-south GPR profile 811. Color scale represents the strength of reflection and phase. The top profile was processed to highlight the top meters. Middle profile is the same as top but with interpretation. The bottom profile was processed to highlight the deeper subsurface down to 20 m. Dashed black lines mark suspected faults mapped in this study.

Vertical resolution can be calculated as a function of the wavelength λ/8 (Widess, 1973) and was found to be ±0.06 m - 0.15 m in this study. Two-way travel time was converted to depth using a measured average velocity of 0.10 m/ns ±0.01 m/ns.

Results of the GPR survey are presented in Figs. 3–8. Depths may vary with ±10% relative to the presented depth scale. The top image shows the un-interpreted data with high-resolution processing that emphasizes the top 0–8 m section. The middle image presents the same profile with interpretation. The bottom sections in each figure were processed to accentuate the deeper subsurface section from about 4 m to an average depth of 18 m. In both representations, numerous suspected faults, marked by black dashed lines, are evident throughout all GPR sections. The study area is located on alluvium and not talus (Fig. 2a and b). It lies within a depression and is surrounded by cover basalt and not material that can slide. For these two reasons and since the study area is adjacent to major fault branches of a plate boundary, we cautiously assume that the vertical lineaments detected on the GPR data are faults and not detachment plains resulting from landslides (e.g. Katz et al., 2009). A interpreted artificial fill is evident Figs. 3c and 4c, down to a maximum depth of around 3 m (light blue dashed line). This was probably laid down to facilitate the construction of the parking lot where the data were collected and the adjacent buildings. As can be seen in all figures, the suspected faults do not cut through this fill. On the other hand, the yellow dashed line (Figs. 3c and 4c) shows that many of these faults reach the bottom of the artificial fill, offsetting the ground beneath by 0.5–0.7 m, which may point to recent activity. The geological map and cross-section (Fig. 2a and b) indicate that the study area lies on a ca. 20 m Holocene alluvium succession underlain by the early Miocene Hordus Conglomerate. Thus, it seems that these lineaments cut through “recent” (Holocene) sediments and may be considered to be

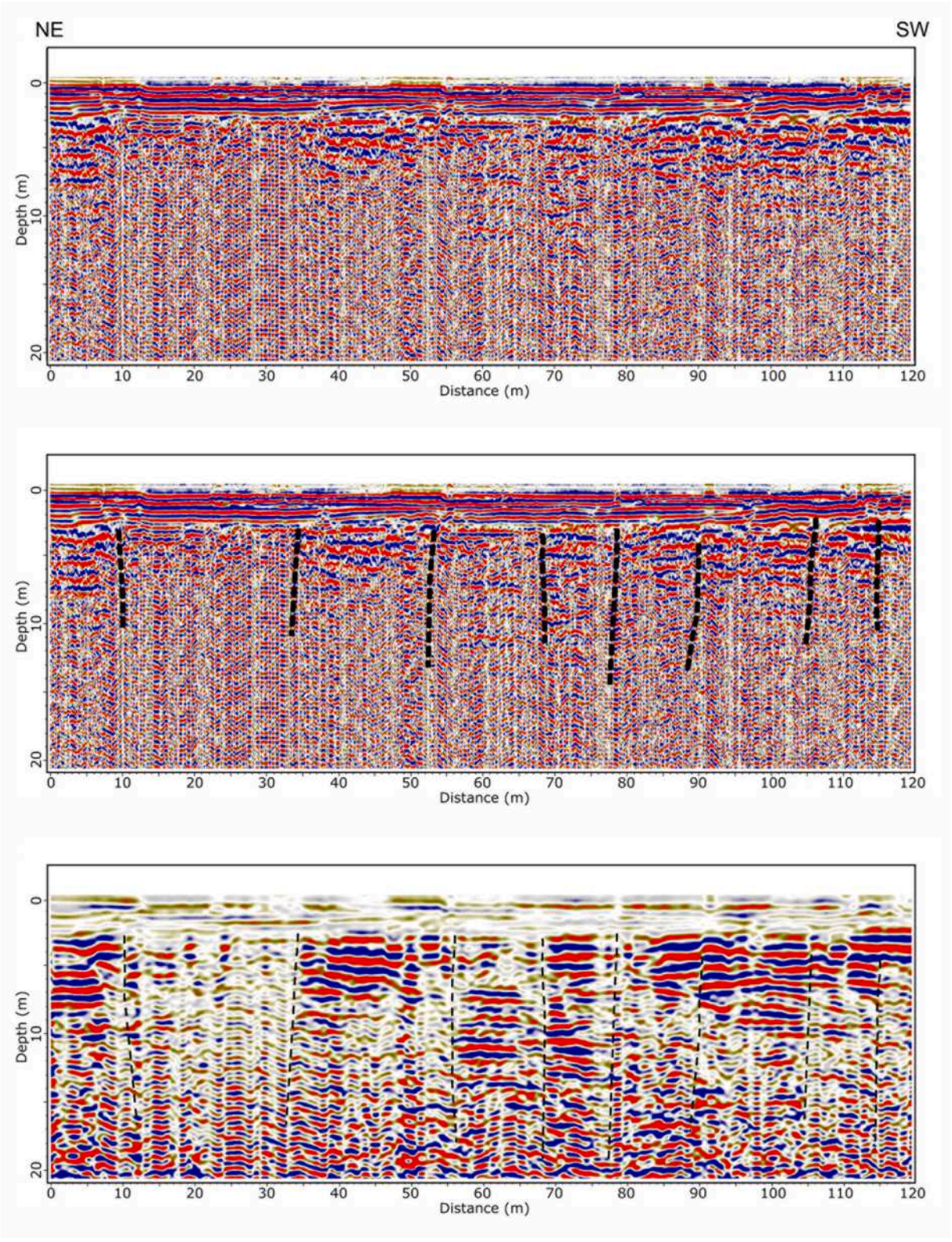

Fig. 7. Northeast-southwest GPR profile 812. Color scale represents the strength of reflection and phase. The top profile was processed to highlight the top meters. Middle profile is the same as top but with interpretation. The bottom profile was processed to highlight the deeper subsurface down to 20 m. Dashed black lines mark suspected faults mapped in this study.

potentially active faults. Fig. 9 presents a configuration of the surface projection (through the ~3 m fill) of all faults recognized in Figs. 3–8. This is one possibility that is based on the orientation and trend of the two major faults that lie some 300 m away from either side of the study area.

Three recent earthquakes mentioned below have been found to have damaged Tiberias, with one leaving clear evidence for surface rupture, one leaving possible evidence and one leaving no evidence. Further to

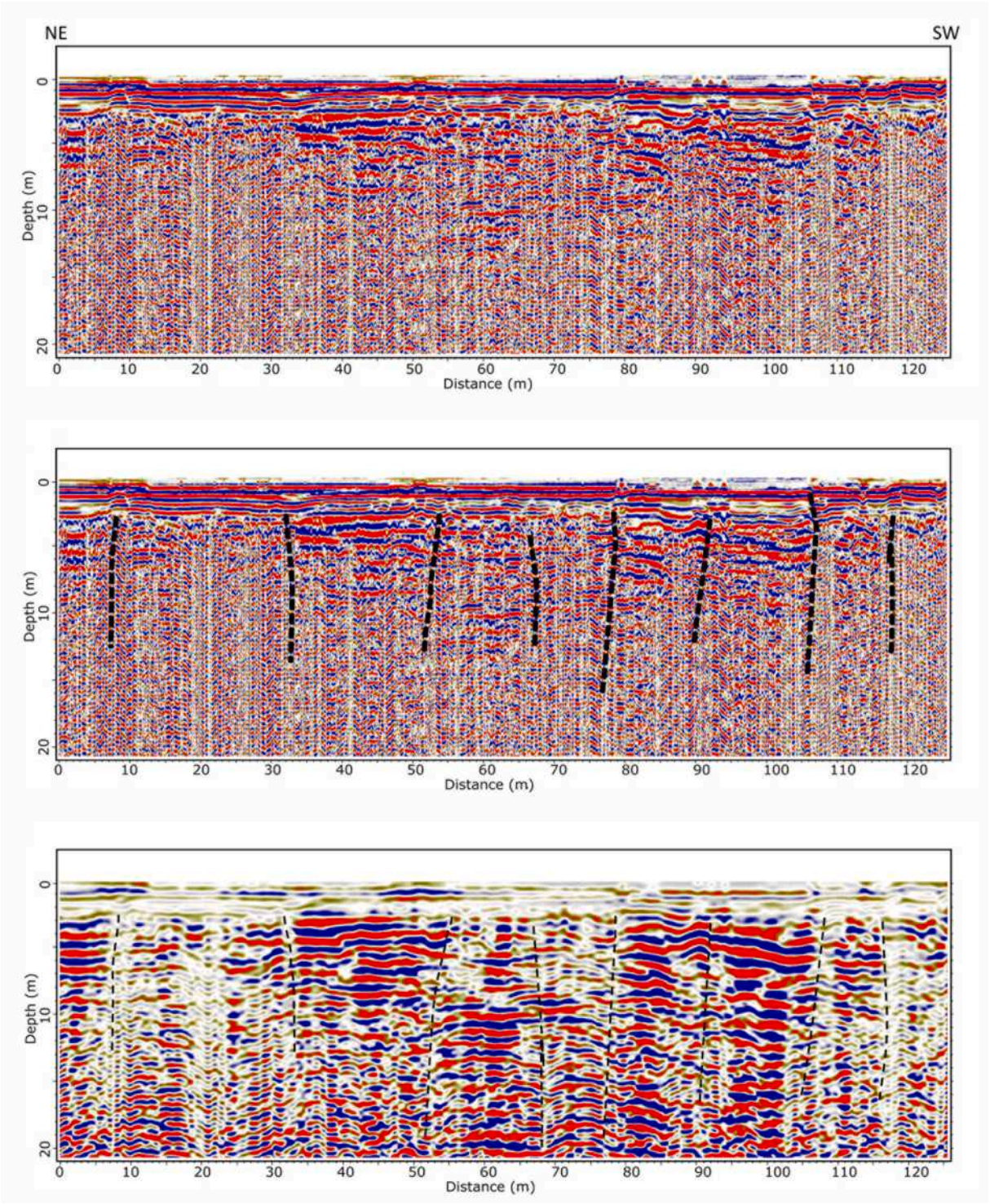

Fig. 8. Northeast-southwest GPR profile 813. Color scale represents the strength of reflection and phase. The top profile was processed to highlight the top meters. Middle profile is the same as top but with interpretation. The bottom profile was processed to highlight the deeper subsurface down to 20 m. Dashed black lines mark suspected faults mapped in this study.

the south of the study area, Ferrario et al. (2020) mapped faults that exhibit vertical offset resulting from the devastating 8th Century earthquakes (with an average magnitude of 7.2; Zohar et al., 2016) that destroyed large parts of the city of Tiberias at that time. The authors attributed this damage to primary surface faulting and concluded by cautiously stating that the western faults, those that cut through Tiberias, perhaps should be considered as major earthquake sources, and not just the eastern boundary fault.

According to Zohar (2016) and Zohar et al. (2016), the 1837 earthquake led to devastating damage and to the complete destruction of most of the dwellings in the city. Its magnitude was assessed to be greater than $M_S > 7$ (Ambraseys, 1997; Zohar et al., 2016) and was probably caused by activity on the Roum fault in Lebanon (e.g. Ambraseys, 1997; Nemer and Meghraoui, 2006). Evidence for surface rupture caused by this earthquake was found to be inconclusive by Ambraseys (1997), while Nemer and Meghraoui (2006) found

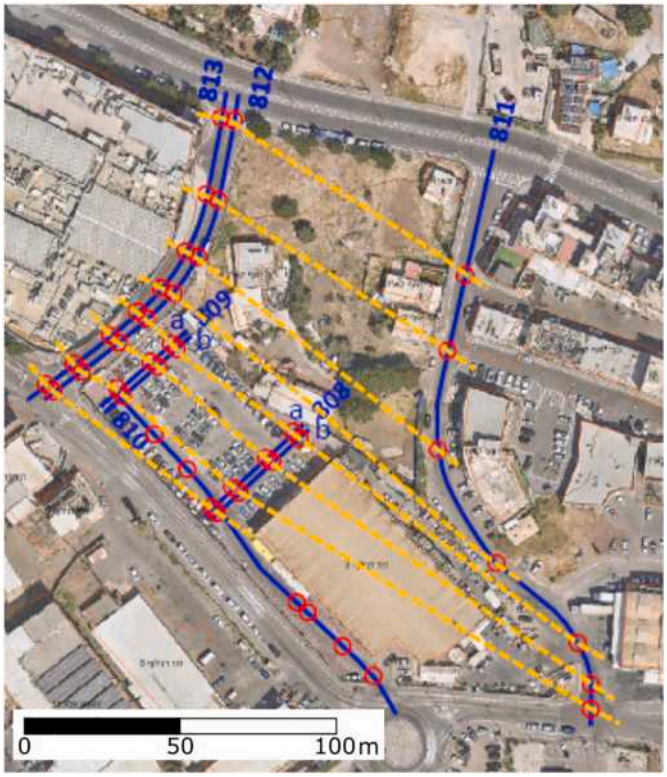

Fig. 9. Interpretation of faults within the study area based on the GPR survey presented above. Red circles mark the location of faults on each of the GPR profiles. Orange lines – possible traces projected onto the surface based on the orientation and trend of the two major faults that lie adjacent to the study area. (For interpretation of the references to color in this figure legend, the reader is referred to the web version of this article.)

indications for possible surface faulting. However, Gasperini et al. (2020) speculated that deformations observed in geophysical data from the Sea of Galilee were formed during this earthquake. According to the authors, rupture should be evident on land around the lake, but little work has been done to find it. Both speculations are based on examination of macroseismic observations, distribution of maximum MSK intensities and fault length versus magnitude.

Finally, the 1927 Jericho earthquake with an average magnitude of 6.25 also caused damage to the city of Tiberias (Zohar et al., 2016). However, this damage was much less extensive than the previous two earthquakes and there is no evidence or suggestion that faults ruptured near the Sea of Galilee. Results of this study indicate that suspected faults cut through Holocene alluvium to reach the base of a modern-day fill. Given the history of recent earthquakes in the area, it could be that these near-surface faults were formed as a result of either earthquakes occurring in the 8th century or in 1837, i.e. the last two major earthquakes that seem to have left their mark on the city. However, more work would need to be done to confirm this speculation.

The current study falls outside the area that should be affected by tectonic motion according to the latest building codes. However, results presented here show that it is riddled with potentially recent faults that probably breached the surface in the past, before the area was developed for commerce. Examination of faults further to the south using a combination of seismic reflection profiles, paleoseismic trenching, archaeological evidence and surface mapping (Ferrario et al., 2020) pointed to the almost fractal nature of faults in the area. What begins as a single fault trace at depth, branches and splays out as it approaches the surface. This behavior has been recognized in numerous studies (e.g. Dooley and McClay, 1997; Basson et al., 2002). Therefore, it is probably incorrect to assume that the location of an active fault on the surface represents the location of the fault at depth. While motion of the main fault at depth can be strike slip, the surface splay may exhibit normal or reverse faulting and is typical of a transtensive environment consistent with that found in the area (Ferrario et al., 2020; Gasperini et al., 2020).

Although construction should not occur anywhere in the vicinity of active or potentially active faults, within the urban environment where land is both scarce and expensive, this cannot always be avoided. In the case of California mentioned above, the APEFZ Act states that the information provided by Earthquake Fault Zones Maps is not adequate. Therefore, cities and counties are obligated to withhold development permits for sites that fall within the defined "earthquake fault zones", i.e. 150–60 m from the fault until geological surveys can establish that there is no threat of future surface rupture or displacement (Bryant and Hart, 2007). In addition, the Act specifically states that active faults may exist outside the Earthquake Fault Zones on any zone map. It provides guidelines for the type of geological and/or geophysical surveys that should be conducted in order to establish the true potential of an area to be active (or not). Note 49 of the APEFZ (Bryant and Hart, 2007) specifies a number of options. The preferred method of investigation is trenching, which allows for direct observation of the faults, should they exist.

As can be seen in Fig. 1c, in the case of modern Tiberias, the city has already expanded to cover areas directly above active and potentially active faults most likely due to construction before the formulation of the building code. The area in between these two faults, which are both main strands of a major plate boundary – the Dead Sea fault, is allocated for a shopping mall and seems to be in the safe zone according to the active fault maps. However, the results of the high-resolution GPR survey carried out here indicate the presence of many potentially active faults. This is despite the overestimation of the potentially hazardous zone set down in the Israeli building code (200 m to either side of a fault) in comparison to other places such as New Zealand (20 m) and California (150–60 m).

Seismic hazard maps, which are used to formulate building codes and locate "safe" zones for construction, should be published with the caveat that any construction plans near active or potentially active faults must be preceded by very high-resolution geophysical surveys, even if these fall inside a seemingly safe zone. In cases such as the one presented in this study where results show suspected faults *outside the zone of active faulting*, trenching or other direct methods of observation should be carried out in order to validate the results. As cities can not stop development due to the presence of active or suspected faults, engineering measures should be planned to enable construction under the strictest safety measures.

CRediT authorship contribution statement

Michael Lazar: Conceptualization, Investigation, Writing – original draft. **Uri Basson:** Methodology, Data curation, Writing – original draft. **Ram Ben-David:** Writing – review & editing. **Judah Coddington:** Writing – review & editing.

Declaration of Competing Interest

The authors declare that they have no known competing financial interests or personal relationships that could have appeared to influence the work reported in this paper.

Acknowledgements

The authors wish to thank GeoSense Ltd. and Roved Geology and Social Consultancy Ltd., for providing some of the data used in this study. We are also grateful to the Editor of Engineering Geology Janusz Wasowski, and two anonymous Reviewers for their helpful comments and suggestions. This research did not receive any specific grant from funding agencies in the public, commercial, or not-for-profit sectors.

References

Aliyannezhadi, A., Mehrnia, S.R., Kimiagar, S., Rahimi, H., Sadrmohammadi, N., 2020. Evaluation of GPR method in identification hidden faults of Alluvial deposits in north of Persian Gulf artificial lake, twenty-two district of Tehran. J. Appl. Geophys. 179, 104108.

Ambraseys, N.N., 1997. The earthquake of 1 January 1837 in southern Lebanon and northern Israel. Ann. Geophys. 4, 923–935.

Ambraseys, N.N., Melville, C.P., 1988. An analysis of the eastern Mediterranean earthquake of 20 May 1202. In: Lee, W.K.H., et al. (Eds.), Historical Seismograms and Earthquakes of the World. Academic Press, San Diego, pp. 181–200.

Anderson, K.B., Spotila, J.A., Hole, J.A., 2003. Application of geomorphic analysis and ground-penetrating radar to characterization of paleoseismic sites in dynamic alluvial environments: an example from southern California. Tectonophysics 368, 25–32.

Basson, U., Enzel, Y., Amit, R., Ben-Avraham, Z., 1994. Detecting and mapping recent faults with ground penetrating radar in the alluvial fans of the Arava Valley, Israel. In: Fifth International Conference on Ground Penetrating Radar, June 12–16, 1994, Kitchener, Ontario, Canada, Vol. 2, pp. 777–788. https://doi.org/10.3997/2214-4609-pdb.300.57.

Basson, U., Ben-Avraham, Z., Garfunkel, Z., Lyakhovsky, V., 2002. Development of recent faulting in the southern Dead Sea Rift according to GPR imaging. In: European Geophysical Society (EGS) Stephan Mueller Special Publication Series, 2, pp. 1–23.

Ben-Avraham, Z., Garfunkel, Z., Lazar, M., 2008. Geology and evolution of the southern Dead Sea fault with emphasis on subsurface structure. Annual Reviews of Earth and Planetary Sciences. https://doi.org/10.1146/annurev.earth.36.031207.124201.

Bogoch, R., Sneh, A., 2008. Geological Maps of Israel 1:50,000 Sheet 4-I: Arbel (Partly Revised, 2014). Israel Geological Survey Jerusalem.

Bryant, W.A., Hart, E.W., 2007. Fault-Rupture Hazard zones in California. Alquist-Priolo Earthquake Fault Zoning Act with Index to Earthquake Fault Zones1 Maps - California Department of Conservation special Publication 42 Interim Revision (41 pp). https://www.cityofdavis.org/home/showpublisheddocument/4411/635803248071430000.

Chow, J., Angelier, J., Hua, J.J., Lee, J.C., Sun, R., 2001. Paleoseismic event and active faulting: from ground penetrating radar and high-resolution seismic reflection profiles across the Chihshang Fault, eastern Taiwan. Tectonophysics 333, 241–259.

Demanet, D., Renardy, F., Vanneste, K., Jongmans, D., Camelbeek, T., Meghraoui, M., 2001. The use of geophysical prospecting for imaging active faults in the Roer Graben, Belgium. Geophysics 66, 78–89.

Dooley, T., McClay, K., 1997. Analog modeling of pull-apart basins. AAPG Bull. 81, 1804–1826.

Ercoli, M., Pauselli, C., Frigeri, A., Forte, E., Federico, C., 2013. Geophysical paleoseismology through high resolution GPR data: a case of shallow faulting imaging in Central Italy. J. Appl. Geophys. 90, 27–40.

Ercoli, M., Pauselli, C., Frigeri, A., Forte, E., Federico, C., 2014. 3-D GPR data analysis for high-resolution imaging of shallow subsurface faults: the Mt Vettore case study (Central Apennines, Italy). Geophys. J. Int. 198, 609–621.

Ferrario, M.F., Katz, O., Hillman, A., Livio, F., Amit, R., Michetti, A.M., 2020. The mid-8 th century CE surface faulting along the Dead Sea Fault at Tiberias (Sea of Galilee, Israel). Tectonics 39 (e2020TC006186).

Gasperini, L., Lazar, M., Mazzini, A., Lupi, M., Haddad, A., Hensen, C., Schmidt, M., Caracausi, A., Ligi, M., Polonia, A., 2020. Neotectonics of the Sea of Galilee (Northeast Israel): implication for geodynamics and seismicity along the Dead Sea Fault system. Sci. Rep. 10, 11932.

Grasmueck, M., 1996. 3-D Ground-penetrating radar applied to fracture imaging in gneiss. Geophysics 61, 1050–1064.

Gross, R., Hollinger, K., Green, A., Begg, J., 2000. 3D ground penetrating radar applied to palaeoseismicity: example from Wellington Fault, New Zealand. In: Noon, D.A., Stickley, G.F., Longstaff, D. (Eds.), Proceedings of the Eighth International Conference on Ground Penetrating Radar, 4084, pp. 478–481.

Haddad, A., Alcanie, M., Zahradnik, J., Lazar, M., Antunes, V., Gasperini, L., et al., 2020. Tectonics of the Dead Sea fault driving the July 2018 seismic swarm in the Sea of Galilee (Lake Kinneret), Israel. Journal of Geophysical Research (JGR): Solid Earth 125. https://doi.org/10.1029/2019JB018963 e2019JB018963.

Hamiel, Y., Piatibratova, O., Mizrahi, Y., 2016. Creep along the northern Jordan Valley section of the Dead Sea Fault. Geophys. Res. Lett. 43, 2494–2501.

Hurwitz, S., Garfunkel, Z., Ben-Gai, Y., Reznikov, M., Rotstein, Y., Gvirtzman, H., 2002. The tectonic framework of a complex pull-apart basin: seismic reflection observations in the Sea of Galilee, Dead Sea transform. Tectonophysics 359, 289–306.

Jol, M., 2009. Ground Penetrating Radar Theory and Applications. Elsevier Science (544 pp).

Katz, O., Amit, R., Yagoda-Biran, G., Hatzor, Y.H., Porat, N., Medvedev, B., 2009. Quaternary earthquakes and landslides in the Sea of Galilee area, the Dead Sea Transform: Paleoseismic analysis and implication to the current hazard. Isr. J. Earth Sci. 58, 275–294.

King, A.B., Brunsdon, D.R., Shephard, R.B., Kerr, J.E., Van Dissen, R.J., 2003. Building adjacent to active faults: A risk-based approach. 2003 Pacific Confrence on Earthquake Engineering Paper #158, p. 8.

Marco, S., Hartal, M., Hazan, N., Lev, L., Stein, M., 2003. Archaeology, history, and geology of the A.D. 749 earthquake, Dead Sea transform. Geology 31, 665–668.

Marco, S., Rockwell, T.K., Heimann, A., Frieslander, U., Agnon, A., 2005. Late Holocene activity of the Dead Sea Transform revealed in 3D palaeoseismic trenches on the Jordan Gorge segment. Earth Planet. Sci. Lett. 234 (2005), 189–205.

Maurya, D.M., Patidar, A.K., Mulchandani, N., Goyal, B., Thakkar, M.G., Bhandari, S., Vaid, S.I., Bhatt, N.P., Chamyal, L.S., 2005. Need for initiating ground penetrating radar studies along active faults in India: an example from Kachchh. Curr. Sci. 88, 231–240.

Maurya, D.M., Chouksey, V., Joshi, P.N., Chamyal, L.S., 2013. Application of GPR for delineating the neotectonic setting and shallow subsurface nature of the seismically active Gedi fault, Kachchh, western India. J. Geophys. Eng. 10, 034006.

Nemer, T., Meghraoui, M., 2006. Evidence of coseismic ruptures along the Roum fault (Lebanon): a possible source for the AD 1837 earthquake. J. Struct. Geol. 28, 1483–1495.

Parliamentary Commissioner for the Environment – PCE, 2001. Building on the edge – the use and development of land on or close to fault lines (ISBN: 0-908804-96-2 38 pp).

Pauselli, C., Federico, C., Frigeri, A., Orosei, R., Barchi, M.R., Basile, G., 2010. Ground Penetrating Radar investigations to study active faults in the Norcia Basin (Central Italy). J. Appl. Geophys. 72, 39–45.

Rashed, M., Kawamura, M.G., Hiroo, N., Miyata, T., Nakagawa, K., 2003. Ground penetrating radar investigation across Uemachi fault, Osaka, Japan. J. Appl. Geophys. 53, 63–75.

Reiss, S., Reicherter, K.R., Reuther, C.-D., 2003. Visualization and characterization of active faults and associated sediments by high-resolution GPR. In: Bristow, C.S., Jol, H.M. (Eds.), Ground Penetrating Radar in Sediments, 211. Geological Society Special Publications, London, pp. 247–255.

Rosensaft, M., Sagy, A., 2019. Active Faults in Israel. GSI WebApp #2/2019, GISunit, Geological Survey of Israel, 2019. https://egozi.gsi.gov.il/webapps/hazards/activefaults/ (Last Accessed 29/7/2021).

Sagy, A., Sneh, A., Rosensaft, M., Bartov, Y., 2016. Map of active faults and potentially active faults for the Israel Standard 413 "design provisions for earthquakes resistance of structures", Update 2016. https://www.gov.il/en/departments/publications/reports/sagy-et-al-report-2016.

Sagy, A., Wieler, N., Avni, Y., Rosensaft, M., Amit, R., 2017. Map of active and potentially active faults that rupture the surface in Israel. In: Updates 2017 for Israel Standard 413. Geological survey of Israel Report N. GSI/13/2017. 20 pp (In Hebrew with English abstract). https://www.gov.il/BlobFolder/reports/sagy-et-al-report2017/he/report_2017_GSI_13_2017.pdf.

Sharon, M., Sagy, A., Kurzon, I., Marco, S., Rosensaft, M., 2020. Assessment of seismic sources and capable faults through hierarchic tectonic criteria: implications for seismic hazard in the Levant. Nat. Hazards Earth Syst. Sci. 20, 125–148.

Sheriff, R.E., 1980. Nomogram for Fresnel-zone calculation. Geophysics 45, 968–972.

Shohet, I.M., Aharonson-Daniel, L., Levi, T., 2016. Analytical-empirical model for the assessment of earthquake casualties and injuries in a major city in Israel - the case of Tiberias. In: Geological Survey of Israel Report No. GSI/21/2016 (85 pp).

Sneh, A., 2008. The Geological Map of Israel, 1:50,000, Sheet 4 II: Teverya. Israel Geological Survey Jerusalem.

Sneh, A., Weinberger, R., 2014. Major geological structures of Israel and environs, scale 1:500.000. Geological Survey of Israel. https://www.gov.il/en/departments/general/geological-stractures-israel-area-embossed.

Standards Institute, 2013. SI 413: Design provisions for earthquake resistance of structures. In: Amendment 5. The Standards Institution of Israel. https://www.iec.co.il/Suppliers/101862470/Amendment%20No%205%20to%20SI%20413.pdf (Last Accessed 27/12/2020).

Utsi, E.C., 2017. Ground Penetrating Radar: Theory and Practice. Butterworth-Heinemann, Amsterdam (225 pp).

Wechsler, N., Rockwell, T.K., Klinger, Y., 2018. Variable slip-rate and slip-per-event on a plate boundary fault: the Dead Sea fault in northern Israel. Tectonophysics 722, 210–226.

Wei, H.-H., Shohet, I.M., Skibniewski, M.J., Shapira, S., Levy, R., Levi, T., Salamon, A., Zohar, M., 2015. Assessment of casualty and economic losses from earthquakes using semi-empirical model. Procedia Engineering 123, 599–605.

Wetzler, N., Shalev, E., Göbel, T., Amelung, F., Kurzon, I., Lyakhovsky, V., Brodsky, E.E., 2019. Earthquake swarms triggered by groundwater extraction near the Dead Sea Fault. Geophys. Res. Lett. 46, 8056–8063.

Widess, M.B., 1973. How thin is a bed? Geophysics 38, 1176–1180.

Zaslavsky, Y., Gorstein, M., Kalmanovich, M., Dan, I., Perelman, N., Giller, D., Ataev, G., Aksinenko, T., Giller, V., Shvartsburg, A., 2009. Site effect and seismic hazard microzonation across the town of Tiberias. In: Geophysical Institute of Israel Report No 502/416/09 (62 pp).

Zhang, D., Li, J., Liu, S., Wang, G., 2019. Multi-frequencies GPR measurements for delineating the shallow subsurface features of the Yushu strike slip fault. Acta Geophysica 67, 501–515.

Zohar, M., 2016. A city hit by an earthquake: an HGIS approach to reconstructing the damage in Tiberias (Israel) in 1837. Int. J. Geogr. Inf. Sci. 31, 81–99.

Zohar, M., Salamon, A., Rubin, R., 2016. Reappraised list of historical earthquakes that affected Israel and its close surroundings. J. Seismol. 20, 971–985.